Liu, D., Lord, O. T., & Flewitt, P. E. J. (2012). Calibration of Raman Spectroscopy in the Stress Measurement of Air-Plasma-Sprayed Yttria-Stabilized Zirconia. Applied Spectroscopy, 66(10), 1204-1209. 10.1366/12-06676

Calibration of Raman Spectroscopy in the Stress Measurement of Air-Plasma-Sprayed Yttria-Stabilized Zirconia

Dong Liu[a,b,*]; Oliver Lord[c,†]; Peter E.J. Flewitt[a,]

[a]Interface Analysis Centre, University of Bristol, Bristol BS2 8BS, UK [b]Department of Mechanical Engineering, University of Bristol, Bristol BS8 1TR, UK [c]School of Earth Sciences, University of Bristol, Bristol BS8 1RJ, UK [d]School of Physics, HH Wills Laboratory, University of Bristol, Bristol BS8 1TL, UK

*Author to whom correspondence should be sent. E-mail: dong.liu@bristol.ac.uk.

Abstract

Thermal barrier coatings (TBC) are used widely on a range of components that operate at high temperatures. We report measurement of the factor that is required to convert the Raman shift to stress for air plasma sprayed yttria (7 wt %) stabilized tetragonal zirconia (ZrO_2) (YSZ) thermal barrier coatings. The factor is evaluated for the as-coated condition and also following a heat treatment at 1000 °C for 1050 h. Two Raman bands at 608 cm^{-1} and 640 cm^{-1} have been investigated in a diamond anvil cell under hydrostatic pressure up to ~24 GPa. In the range of zero to ~1.6 GPa, a linear behavior was observed in terms of the shifts of these two Raman bands with a gradient similar to dense bulk tetragonal ZrO_2. From these measurements the factors to convert wavenumber shift to stress have been derived. The application of these conversion factors to stress measurement in TBC coated test specimens and components is discussed.

Index Headings
Raman spectroscopy,
Conversion factor,
Air plasma spray,
Tetragonal yttria-stabilized zirconia,
Stress

Introduction

Stress analyses of ceramic materials have been reported that deal with the determination of residual and applied stresses using spectroscopic techniques based on the Raman piezospectroscopic (PS) effect.[1–3] Stress changes the frequency of the vibrational modes of the ceramic lattice and thus the wavenumber of the Raman bands. The factor used to relate Raman shift to residual stress is a pre-requisite for the application of this technique to the determination of stress. Any PS characterization aiming to use a Raman effect in ceramics must start with precise, case-by-case calibration procedures.[1] Thin air-plasma-sprayed yttria-stabilized zirconia (APS-YSZ) thermal barrier coatings (TBC) are widely used on turbine blades to sustain an appreciable temperature difference, allowing operation at high temperatures. The physical properties of the TBC depend upon both the composition and the microstructure.[1] These coatings normally consist of three layers: an outer ceramic coating and a metallic bond coat that provides good adherence of the ceramic coating to the underlying substrate. The third layer (predominately Al_2O_3) develops between the ceramic coating and the bond coat during exposure at the service temperature and is termed the thermally grown oxide (TGO) layer.[4] The growth of this oxide is one of the factors that contributes to the spallation of the TBC in the later stages of service life. To be able to evaluate the life of coated turbine blades, it is important to measure the progressive change in residual stresses in the TBC and TGO layers. Therefore, the calibration of the PS Raman effect with respect to the externally applied stress and internally generated secondary residual stress requires consideration of the specific microstructure for the material under investigation.

There are published conversion factors for dense bulk tetragonal zirconia, including yttria stabilized zirconia (YSZ) and pure tetragonal zirconia[5,6] under both uniaxial[7] and hydrostatic[5] external loading. However, well-established calibration factors for APS-YSZ coatings have not yet been determined[3,5,6,8–10] despite the fact that APS-YSZ is widely used on turbine blades. In addition, little consideration has been given to potential changes that may arise as a consequence of exposure to service conditions. In this paper, the conversion factor for APS-YSZ in the as-sprayed and a simulated service-exposed condition have been investigated.

Experimental

The starting materials for these experiments are APS-YSZ on a single crystal CMSX4 super alloy substrate with an intermediate Amdry 995 bond coat in the as-coated condition and a second specimen heat-treated for 1050 h at 1000 °C. Two micro-scale specimen disks with a diameter of ~100 μm and a thickness of ~30 μm were cut from both APS-YSZ specimens using an ultraviolet laser ablation system. Hydrostatic stresses were applied to the specimens using a diamond anvil cell (DAC). The arrangement is shown schematically in Fig. 1a and a general view of the DAC is shown in Fig. 1b. Each specimen was loaded into a 150 μm diameter sample chamber created by drilling a hole in a stainless steel gasket pre-indented to a thickness of ~50 μm and mounted on the lower of the two opposing diamond anvils (Fig. 1a). The remaining space in the

sample chamber was then filled with a 4:1 methanol:ethanol mixture as the hydrostatic pressure medium,[11] together with a few ruby grains (with a grain size of 1 to 3 μm) as an internal pressure standard. For each loading step, the pressure in the chamber was measured by photo-stimulated luminescence piezo-spectroscopy (PLPS) emission from the ruby grains according to the calibration undertaken by He and Clarke.[12] Since the conditions within the DAC were hydrostatic, the constant 7.61 cm^{-1} GPa^{-1} for the R2 (14432 cm^{-1}) peak shift was used. The shifts of the Raman peaks were recorded at the same time to determine the conversion factor. Under each loading condition, 3 to 5 locations around the specimen were investigated and at each location 3 spectra were acquired to check both the experimental uncertainty and the variation of the stress around the specimens. Therefore, for each stress point, 9 to 15 measurements undertaken on the specimen were averaged and the standard deviation plotted as an error bar. A long working distance (LWD) Olympus lens with a 50× magnification and a numerical aperture of 0.55 was used when acquiring the spectra.

The cross-section of the APS-YSZ, presented in Fig. 2a, shows the complex microstructure and Fig. 2b shows typical Raman spectra for APS-YSZ. The measurements were made using a Renishaw Ramanscope spectrometer, model 2000, fitted with a laser source with a wavelength, λ, of 632.8 nm and an integrated microscope that allows the observation of the specimen surface. The peaks were fitted using a mixed Gaussian and Lorentzian method after the removal of the background.[12] The peaks centered at 608 cm^{-1} and 640 cm^{-1} were selected for measurement and calibration because of their large signal-to-noise ratio and pronounced intensity. The other peaks as shown in Fig. 2b have significantly reduced intensity at many locations in both the as-coated and heat-treated specimens. It was noteworthy that most of the spectra collected during these experiments included the full six-peak tetragonal zirconia pattern, whereas at some locations there was a reduced intensity of peaks located within the lower frequency range. This scenario limits the application of the peak centered at 465 cm^{-1} for calibration of APS-YSZ as proposed by Limarga et al.[13] based on bulk dense pure YSZ material.

Results

Loading Response of APS-YSZ

In the first experimental run, the as-coated APS-YSZ specimen was loaded to a compressive stress of ~14 GPa, unloaded slowly to zero, and then reloaded to ~24 GPa.[‡] The aim of these repeated cycles of loading and unloading was to establish whether any deformation damage was introduced into the APS-YSZ during the first loading cycle. The hydrostatic stress-induced shift of the Raman peak centered at 640 cm^{-1} is plotted in Fig. 3. At low stress, the Raman shift follows a linear response to applied hydrostatic stress, but at high stress the response indicates a nonlinear elastic behavior as observed in macro-scale testing.[14,15] No hysteresis or plasticity was observed during the repeat loading, unloading, and reloading cycles.

The linear relationship found between the externally applied stress and Raman shifts at low range is consistent with the behavior of pure, dense bulk YSZ material.[5–7,10,16] Elastic stiffening of the material with increasing stress was observed at values above ~15 GPa. This may be due to the consolidation of the specimen by the closure of flaws and pores. Certainly it is one of the distinct characteristics reported for structured tetragonal zirconia compared with pure bulk YSZ.[2,17] In addition, a reversible phase transformation from tetragonal zirconia to cubic zirconia was observed in this experiment at ~15 GPa, which is higher than the 8 GPa transition pressure reported for undoped tetragonal zirconia.[2] We defined the appearance of the cubic zirconia phase in terms of the sudden increase in intensity of a peak centered at ~570 cm^{-1} and the more pronounced intensity at ~610 cm^{-1}.[6] The higher transition stress level is consistent with the fact that the microstructure of the YSZ accommodates part of the externally applied stress together with enhanced stability of the tetragonal phase.

In general, the nonlinear elasticity response of APS-YSZ at high stresses recovered elastically and did not introduce any obvious damage within the lower loading range. This covers the range of interest for the measurement of TBC stresses, which is normally lower than 1.5 GPa.[13,18] Therefore, in the second experimental run, an as-coated specimen was heat-treated for 1000 h at 1050 °C, then loaded from zero to ~1.6 GPa and unloaded to zero in small steps to establish the Raman conversion factor. The Raman shifts both for 608 cm^{-1} and 640 cm^{-1} peaks show a linear response with the increase of hydrostatic stress as shown in Figs. 4a and 4b.

An unavoidable issue in this experimental work, which may contribute to the stiffening in as-coated specimens under high stress, is that when the pressure in the DAC exceeded about 10 GPa, the liquid mixture transformed into an amorphous solid state so that the stress state was no longer purely hydrostatic.[11] Non-hydrostatic stresses can create inhomogeneous strain in a crystal and this is reflected in the broadening of the R1 and R2 ruby peaks as the loading conditions changed in the DAC as shown in Fig. 5. The two ruby peaks (R1: 14400 cm^{-1}, R2: 14432 cm^{-1}) have a stable full width at half-maximum (FWHM) as the stress increased, but they significantly broaden when the stress reaches ~10 GPa. This indicates that the introduction of anisotropic stress conditions results in stress along the diamond loading axis that is not exactly the same as the stress in the plane perpendicular to the diamond loading axis. Gadag et al.[19] suggested that it is difficult to precisely quantify the anisotropy, especially if the crystal is not cubic. However, ruby is a relatively stiff material with a bulk elastic modulus of about 254 GPa,[20,21] so it is intrinsically less sensitive to non-hydrostatic components of stress. The stress in the DAC, therefore, was still calculated using the hydrostatic factor of 7.61 cm^{-1} GPa^{-1} even when the value was in excess of 10 GPa. This approximation will tend to minimize the stiffening trend for the YSZ at higher stresses.

Raman Conversion Factor

In the application of Raman spectroscopy to TBCs formed by air plasma spraying of YSZ, the stresses of interest are normally less than 1 GPa and are in the linear range of the loading curve (Fig. 3). The externally applied hydrostatic stress, σ, is calculated using the following relationship:

$$\sigma_{ij} \text{ 1/4 } \upsilon_{ij}=\Pi_{ij}$$

where Δv is the Raman shift of the peak (cm^{-1}) from the stress free state and Π is the conversion factor. We consider only the principal stress tensor in this hydrostatic loading environment. Shifts to a higher frequency indicate a compressive stress.

The factor to convert the Raman shift to stress was quantified for both the as-coated and heat-treated specimens tested (Fig. 4). The peak at 608 cm^{-1} yielded Π values of 5.07 ± 0.1 $GPa^{-1}\cdot cm^{-1}$ for as-coated APS-YSZ and 5.05 ± 0.1 $GPa^{-1}\cdot cm^{-1}$ for heat-treated material (Fig. 4a). By comparison, the peak at 640 cm^{-1} is related to externally applied stress by a Π value of 5.55 ± 0.1 $GPa^{-1}\cdot cm^{-1}$ for the as-coated APS-YSZ and 5.65 ± 0.1 $GPa^{-1}\cdot cm^{-1}$ for the heat-treated (Fig. 4b). There are a range of values that have been reported previously for tetragonal zirconia material in different conditions. Teixeira et al.[10] presented a linear relationship between the applied tensile stress and the Raman shift and proposed that each shift equals 220 MPa,[22] which indicates a conversion factor of 4.54 $GPa^{-1}\cdot cm^{-1}$. This value is fairly close to the value of 5.55 ± 0.1 $GPa^{-1}\cdot cm^{-1}$ obtained for the 640 cm^{-1} wavenumber peak in this contribution. However, Teixeira did not provide detail for the loading and measurement system used. Other factors reported vary with the materials tested and the loading approach applied. For example, Tanaka et al.[23] gave a uniaxial factor of 25 $GPa^{-1}\cdot cm^{-1}$ by loading a free-standing 8 wt % YSZ manufactured by APS, whereas Cai et al.[6] obtained a uniaxial value of 1.1 $GPa^{-1}\cdot cm^{-1}$ for dense yttria-stabilized cubic polycrystalline zirconia. For bulk dense materials under hydrostatic loading conditions, the variation in the conversion factors diminishes such that Alzyab et al.[8] acquired a value of 3.2 $GPa^{-1}\cdot cm^{-1}$ for 5 wt % YSZ and Bouvier et al.[5] reported 2.79 $GPa^{-1}\cdot cm^{-1}$ for nanometric tetragonal zirconia. These values are significantly different for the APS-YSZ because they used single crystals and powdered specimens, respectively. Considering the results in this contribution, the factor given for the 608 cm^{-1} peak is smaller than that given by the 640 cm^{-1} peak and this trend is in agreement with data obtained previously.[5–7]

The sintering of APS-YSZ by heat treatment has been reported to cause a change in the elastic modulus obtained by nano-indentation, which is a uniaxial compressive loading deduced modulus.[24,25] In the present specimens, the sintering leads to linking of micro-cracks and splat boundaries to form larger cracks and boundaries together with a reduction in porosity. The current test considers the compliance of the material under hydrostatic pressure. The selected heat treatment of 1000 °C for 1050 h provides an APS-YSZ microstructure that is judged to bound the severe thermal history experienced by TBC coated blades in land-based gas turbines during service.[26] A nano-indentation test carried out on the heat-treated specimen validated that the sintering has completed since the elastic modulus values compare with the fully sintered data. Despite the changes in the elastic modulus and microstructure, the conversion factor remains

unchanged within experimental error so that a single value can be used to measure stresses over the service life of coated turbine blades.

The application of this conversion factor to the measurement of residual stress on components or test specimens is a reversed process of the calibration. The Raman shifts are measured and stress is deduced from the parameters obtained from the linear curves in Figs. 4a and 4b. Hence, it is important to consider differences in the conditions of externally applied stress used in the calibration and intrinsic residual stresses in a test specimen together with the sampled volume. Residual stress is a secondary stress so that there is no displacement of the body.[27] The information collected from Raman spectra is a description of the average stress state of the material in the probed volume. As shown by the present workers there is dispersion of the incident laser beam within the APS-YSZ to produce a cone-shaped volume so that the beam increases from an initial 1.5 μm diameter to ~35 μm diameter at a depth of ~40 μm.[28] Thus, splat boundaries, pores, and other micro-scale flaws are contained within a typical sampled volume. A mix of nano-scale columnar prismatic and equiaxed YSZ grains is contained within the splats as shown in Fig. 6. The length of the prismatic grains is ~500 nm, and the size of the equiaxed grains varies from 50 nm to 200 nm in diameter. Both the intra-granular and inter-granular defects were observed at the fracture surface. Considering the large number of grains sampled, the orientation of unit cells can therefore be assumed to be isotropic, and the stress to be in a multi-axial state. Therefore, the hydrostatically calibrated conversion factors can be readily applied to gain the hydrostatic stress level in the probed volume. However, it should be noted that the stress calculated from the Raman shifts represents the average of the multi-axial local stress in the probed volume. It cannot be used to determine whether the whole YSZ layer is in a biaxial, uniaxial, or hydrostatic state. The macro-scale stress state of the layer is defined by macro-scale elasticity theory.[27] For example, in TBCs, where the YSZ layer is ~200 μm thick and the substrate is of the order of centimeters thick, linear elastic generalized plane stress theory is normally adopted to assume that the YSZ is in the biaxial stress state.

Conclusions

In summary, the factors to convert wavenumber shifts to stress in Raman spectroscopy have been evaluated for peaks at 608 cm^{-1} and 640 cm^{-1} for both as-coated and thermally aged APS-YSZ. These factors obtained from the 640 cm^{-1}peak are 5.65 $GPa^{-1}\cdot cm^{-1}$ for as-coated and 5.55 $GPa^{-1}\cdot cm^{-1}$ when heat-treated at 1000 °C for 1050 h. The corresponding values for the peak at 608 cm^{-1} are 5.07 $GPa^{-1}\cdot cm^{-1}$ and 5.05 $GPa^{-1}\cdot cm^{-1}$, respectively. Taking into account the experimental error of ±0.1 $GPa^{-1}\cdot cm^{-1}$ together with the good repeatability of this calibration, we conclude that thermal aging does not affect the Raman conversion factor. In addition, the response is linear over the range up to 10 GPa, thereby giving confidence when making measurements of stress up to this value. The use of a single conversion factor provides confidence in the measurement of stresses within TBC coated components subject to a range of thermal exposures typical of those encountered in service of land-based gas turbines.

Acknowledgements

We would like to acknowledge the support of The Energy Programme, which is a Research Councils UK cross council initiative led by EPSRC and contributed to by ESRC, NERC, BBSRC, and STFC, and specifically the Supergen initiative (Grants GR/S86334/01 and EP/F029748) and the following companies: Alstom Power Ltd., Doosan Babcock, E.ON, National Physical Laboratory, Praxair Surface Technologies Ltd., QinetiQ, Rolls-Royce plc, RWE npower, Siemens Industrial Turbomachinery Ltd., and Tata Steel, for their valuable contributions to the project. OTL would like to acknowledge support from NERC grants NE/F019084/1 and NE/H003541/1.

Notes

†Present address: Department of Earth Sciences, University College London, London WC1E 6BT, UK.

†Since all stresses considered in this paper are compressive the notation of plus is assigned arbitrarily.

References

1. Giuseppe P. In Situ Study of Fracture Mechanisms in Advanced Ceramics Using Fluorescence and Raman Microprobe Spectroscopy". J. Raman. Spectrosc. 1999;30(10):867–75.
2. Bouvier P., Djurado E., Lucazeau G., Bihan. " T.L. High-pressure Structural Evolution of Undoped Tetragonal Nanocrystalline Zirconia. Phys. Rev. B. 2000;62(13):8731–7.
3. Limarga A.M., Clark D.R. Piezo-Spectroscopic Coefficients of Tetragonal-Prime Yttria-Stabilized Zirconia. J. Am. Ceram. Soc. 2007;90(4):1272–5.
4. Miller R.A., Lowell C.E. Failure Mechanisms of Thermal Barrier Coatings Exposed to Elevated Temperatures. Thin. Solid. Films. 1982;95(3):265–73.
5. Bouvier P. G. Lucazeau. "Raman Spectra and Vibrational Analysis of Nanometric Tetragonal Zirconia under High Pressure. J. Phys. Chem. Solids. 2000;61(4):569–78.
6. Cai J.G., Raptis Y.S., Anastassakis E. Stabilized Cubic Zirconia—a Raman-Study under Uniaxial-Stress. Appl. Phys. Lett. 1993;62(22):2781–3.
7. Limarga A.M., Clarke D.R. Piezo-Spectroscopic Coefficients of Tetragonal-Prime Yttria-Stabilized Zirconia. J. Am. Ceram. Soc. 2007;90(4):1272–5.
8. Alzyab B., Perry C.H., Ingel R.P. High-pressure Phase Transitions in Zirconia and Yttria-Doped Zirconia. J. Am. Ceram. Soc. 1987;70(10):760–5.
9. Sergo V. Room-Temperature Aging of Laminate Composites of Alumina/3-mol%-Yttria-Stablilized Tetragonal Zirconia Polycrystals. J. Am. Ceram. Soc. 2004;87(2):247–53.
10. Teixeira V., Andritschky M., Fischer W., Buchkremer H.P., Stover D. Analysis of Residual Stresses in Thermal Barrier Coatings. J. Mater. Process. Technol. 1999;93(1):209–16.
11. Angel R.J., Bujak M., Zhao J., Gatta G.D., Jacobsen S.D. Effective Hydrostatic Limits of Pressure Media for High-Pressure Crystallographic Studies. J. Appl. Crystallogr. 2007;40(1):26–32.
12. He J., Clarke D.R. Determination of the Piezospectroscopic Coefficients for Chromium-Doped Sapphire. J. Am. Ceram. Soc. 1995;78(5):1347–53.
13. Limarga A.M., Vassen R., Clarke D.R. Stress Distributions in Plasma-Sprayed Thermal Barrier Coatings Under Thermal Cycling in a Temperature Gradient". J. Appl. Mech.-T. ASME. 2011;78(1):011003–11.
14. Zhu D., Miller R.A. Investigation of thermal fatigue behavior of thermal barrier coating systems. Surf. Coat. Tech. 1997;94-95(0):94—101.
15. Echsler H., Renusch D., Schütze M. Mechanical Behaviour of As Sprayed and Sintered Air Plasma Sprayed Partially Stabilised Zirconia. Mater. Sci. Tech. 2004;20(7):869–76.
16. Mao W.G., Chen Q., Dai C.Y., Yang L., Zhou Y.C., Lu C. Effects of piezo-spectroscopic coefficients of 8 wt.% Y2O3 stabilized ZrO2 on residual stress measurement of thermal barrier coatings by Raman spectroscopy. Surf. Coat. Tech. 2010;204((21-22)):3573–7.
17. Zhu D., Miller R. Thermal Conductivity and Elastic Modulus Evolution of Thermal Barrier Coatings Under High Heat Flux Conditions". J. Therm. Spray. Technol. 2000;9(2):175–80.

18. Liu D., Flewitt P.E.J., Hallam K.R. The Measurement of Residual Stresses in Thermal Barrier Coated Model Aerofoils. Key. Eng. Mater. 2012;488-489(1):9–12.
19. Gadag S., Subbarayan G. , W. Barker. “Thermo-elastic Properties of Dense YSZ and Porous Ni-ZrO2 Monolithic and Isotropic Materials. J. Mater. Sci. 2006;41(4):1221–32.
20. Richet P., Xu J.A., Mao H.K. Quasi-hydrostatic Compression of Ruby to 500 Kbar. Phys. Chem. Miner. 1988;16(3):207–11.
21. Zajonz J.K., Werner S., Schulz H. High Pressure Single Crystal X-ray Diffraction Study on Ruby Up to 31 GPa. Z. Krist- New Cryst. St. 1999;214(6):331–6.
22. Portinha A., Teixeira V., Carneiro J., Beghi M.G., Bottani C.E., Franco N., Vassen R., Stoever D., Sequeira A.D. Residual stresses and elastic modulus of thermal barrier coatings graded in porosity. Surf. Coat. Tech. 2004;188:120–8.
23. Tanaka M., Hasegawa M., Dericioglu A.F. Y. Kagawa. “Measurement of residual stress in air plasma-sprayed Y2O3–ZrO2 thermal barrier coating system using micro-Raman spectroscopy. Mater. Sci. Eng. A. 2006;419((1–2)):262–8.
24. Zhu D.M., Choi S.R., Miller R.A. Sintering and Fracture Behavior of Plasma-Sprayed Thermal Barrier Coatings. The 106th Annual Meeting and Exposition to the American Ceramic Society. 2004 India.
25. Cipitria A., Golosnoy I.O., Clyne T.W. A Sintering Model for Plasma-sprayed Zirconia Thermal Barrier Coatings. Part II: Coatings Bonded to a Rigid Substrate. Acta Mater. 2009;57(4):993–1003.
26. Hilson G. “The Inter-relationship Between Surface Condition and Near Surface Residual Stresses in Engineering Components”. PhD Thesis. Bristol, UK: University of Bristol; 2008.
27. Boresi A.P., Schmidt R.J. InBoresi A.P., Schmidt R.J. editorsAdvanced Mechanics of Materials. John Wiley and Sons; 2003 6th Edition. pp.
28. Liu D., Lord O., Stevens O., Flewitt P.E.J. The Role of Beam Dispersion within YSZ in the Application of Raman and Photo-Stimulated Luminescence Piezo-Spectroscopy in Multi-layered Coatings. Submitted for publication. 2012.

FIG. 1.

(**a**) The schematic arrangement of the diamond loading system and (**b**) the general view of the diamond anvil cell.

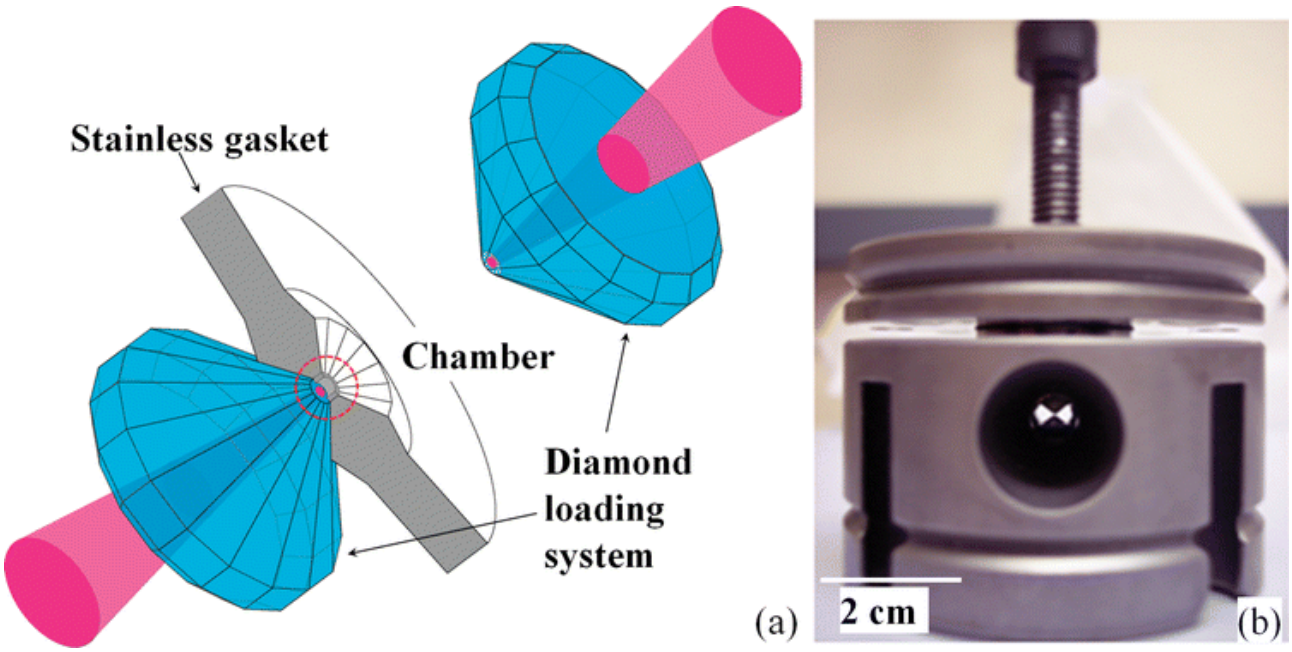

FIG. 2.

APS-YSZ (**a**) scanning electron micrograph showing as-coated cross-section microstructure, and (**b**) typical Raman spectra of tetragonal zirconia together with a spectrum showing the disappearance of the Raman peaks in the range 100 cm^{-1} to 500 cm^{-1}.

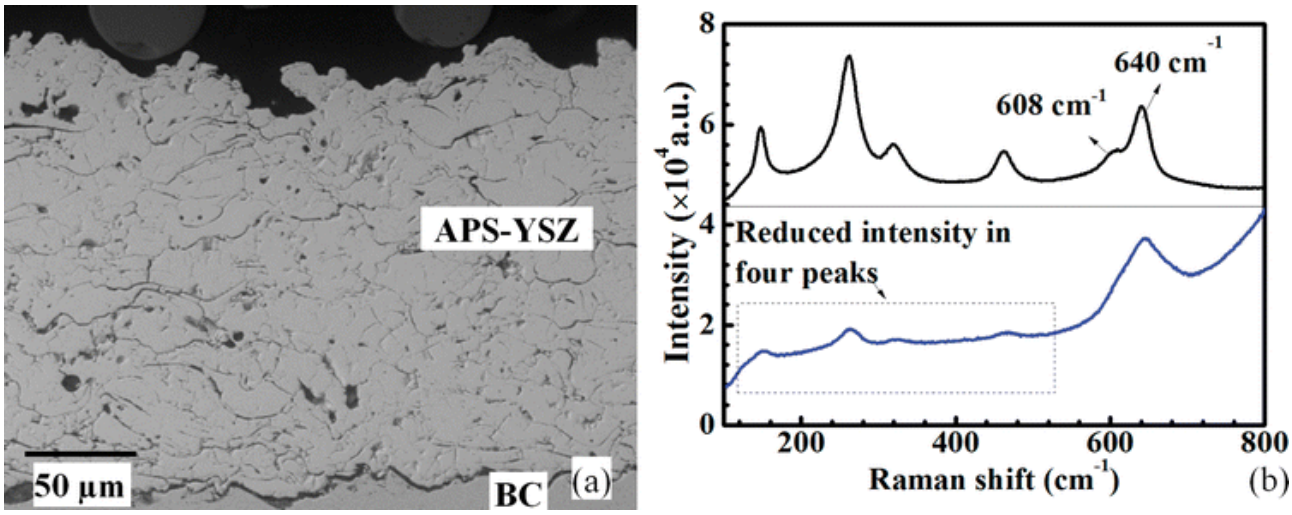

FIG. 3.

Shift of the 640 cm $^{-1}$ Raman peak of the as-coated specimen subjected to hydrostatic stress.

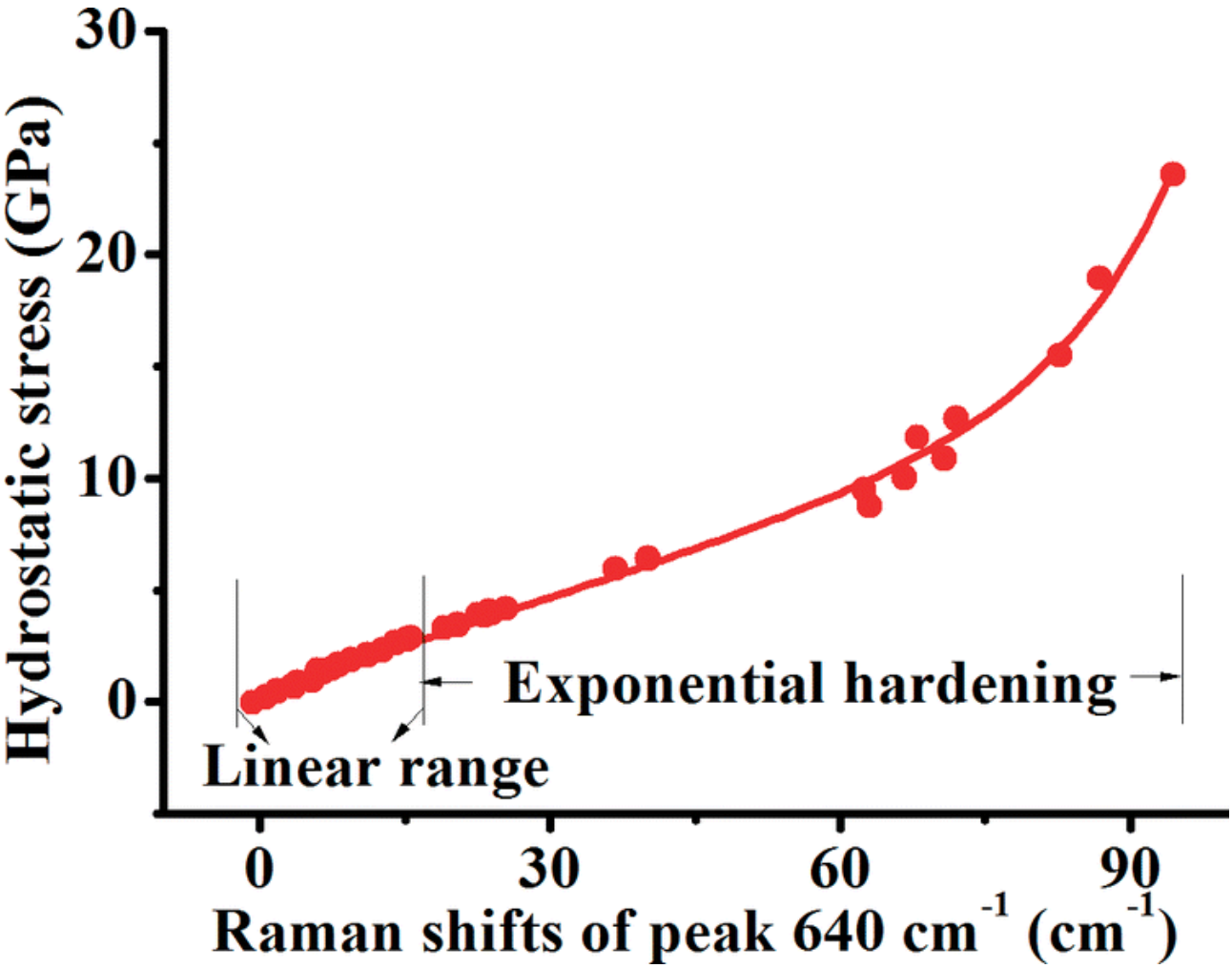

FIG. 4.

The shifts of (**a**) the 608 cm $^{-1}$ peak and (**b**) the 640 cm $^{-1}$ peak for TBC specimens subject to hydrostatic stress.

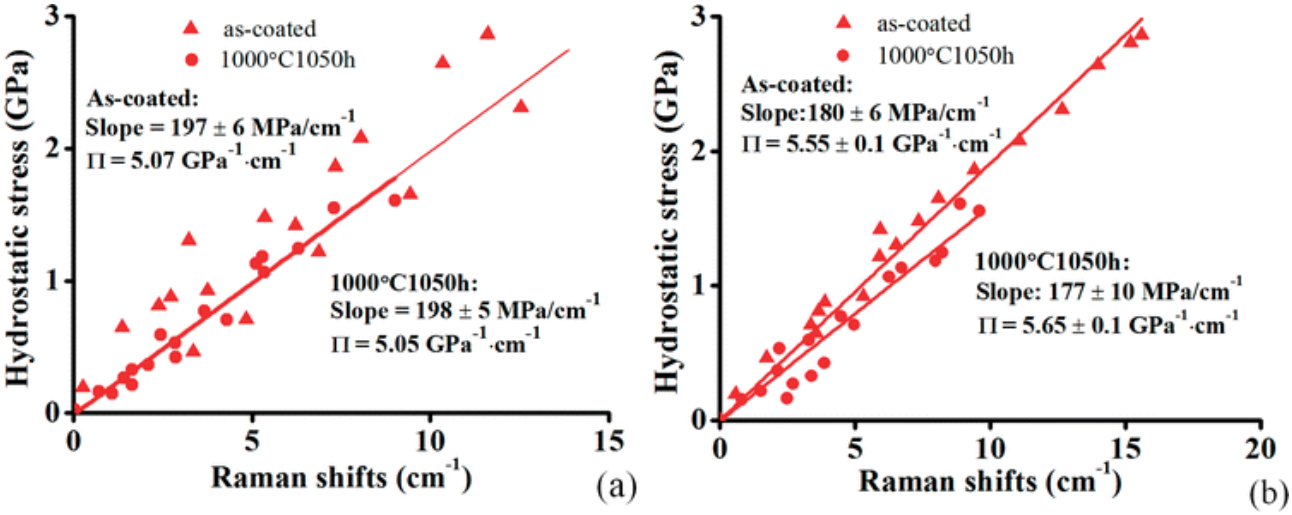

FIG. 5.

R1 and R2 peak broadening on loading, unloading, and reloading cycles.

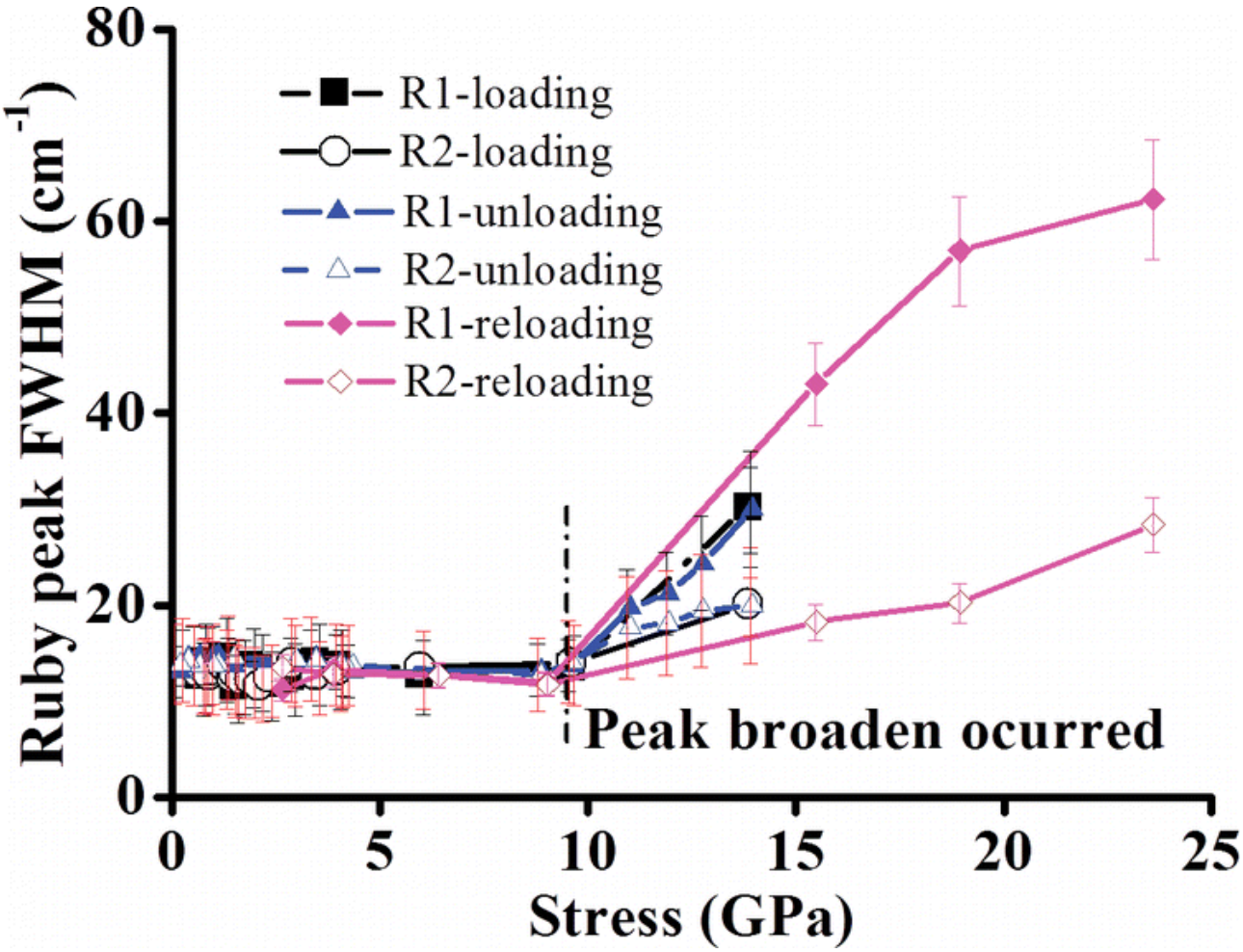

FIG. 6.

Scanning electron image of a fracture surface revealing both prismatic and equiaxed zirconia grains.